Controlling amorphous silicon in scratching for fabricating high-performance micromixers

Tingting Chen[1], Licong Cui[1], Wang He[1], Renxing Liu[1], Chengqiang Feng[1], Lei Wu[1], Yang Wang[2], Huiyun Liu[3], Linmao Qian[1], Bingjun Yu[1,*]

[1] Tribology Research Institute, School of Mechanical Engineering, Southwest Jiaotong University, Chengdu 610031, China

[2] Academy of Frontier Sciences, Southwest Jiaotong University, Chengdu 610031, China

[3] Department of Electronic & Electrical Engineering, University College London, Torrington Place, London WC1E 7JE, U.K.

* Email: bingjun@swjtu.edu.cn, Tel.: +86 28 87634181, Fax: +86 28 87603924

ABSTRACT

As core parts of microfluidic chip analysis systems, micromixers show robust applications in wide fields. However, restricted by the fabrication technology, it remains challenging to achieve high-quality micromixers with both delicately designed structure and efficient mixing. In this study, based on the theory of chaotic mixing, sinusoidal structures with variable phase were designed and then fabricated through scanning probe lithography (SPL) and post-selective etching. It is found that the scratches with phase difference can lead to the periodic formation of amorphous silicon (a-Si), which can resist against the etching. Consequentially, misaligned sine channels with thick-thin alternate 3D shapes can be generated in-situ from the scratching traces after the etching. Further analysis showed that thicker a-Si layer can be obtained by reducing the line spacing in the scratching, confirmed by Raman detections and simulations. With the proposed method, the misaligned sine micromixer was achieved with higher mixing efficiency than ever. The duplicating process was also investigated for high-precision production of micromixers. The study provided strategies for the miniaturization of high-performance microfluidic chips.

Keywords: Sinusoidal micromixers; Mixing efficiency; Selective etching; Amorphous silicon

1. Introduction

The micromixer is a kind of reactor for mixing two or more liquids in designed channel at the microscale, which is broadly utilized in biology, chemistry, medical fields, and so on.[1] For instance, efficient mixing of anticoagulants and chemical reagents is necessary for accurately detecting bacteria and viruses.[2] Adequately mixing templates, primers, enzymes, and deoxyribonucleotide triphosphates (DNTP), in the process of polymerase chain reaction (PCR), is desired for speedy amplification.[3] Additionally, rapid mixing is also significant for microfluidic chips to play roles in DNA hybridization, nucleic acid detection, and drug delivery.[4,5] Accordingly, the improvement in the efficiency of micromixers has received attention worldwide.[6,7] However, since the Reynolds number of microchannels at less than 500 is laborious to bring about liquid disturbance,[8] it remains challenging to increase the efficiency of ordinary microchannels, which hinders its extensive applications.

The improved mixing efficiency of active and passive micromixers has aroused intense research interest.[9,10] Actively placing extra electric, magnetic, or thermal fields outside micromixers is a popular method to interfere with fluids and enhance diffusion rate.[11-13] Although external fields can promote mixing efficiency, the charged performance or magnetism of the fluid is required for active micromixers, which makes it unsuitable for all fields.[14] By contrast, the passive micromixer with asymmetric structures can boost the mixing efficiency,[15-19] and hence present wider applications than active ones.[20] A striking example is that the optimum winglet angle of asymmetric

barriers, accessed by simulating, can improve the mixing efficiency by at least 25%.[21] Since the secondary flow capable of accelerating the mixing of two-phase flows is rare in rectangular, zigzag, and circular arc structures but frequent in serpentine channels, the formers exhibit relatively low mixing efficiency.[22,23] It's also noted that the micromixer with sinusoidal structure, appearing in several study cases, can facilitate the mixing.[24,25] In summary, designing three-dimensional (3D) mixer shapes for enhancing the efficiency over short flow distances remains challenging, which is essential for miniaturizing microfluidic chips and increasing detection accuracy and rate in chips.

After the design of structure is completed, how to convert the concept into the production usually becomes a tough challenge for achieving complex channels. Many practical techniques have been applied to realize various microchannels. 3D printing, a relatively new, yet successful approach to forming microfluidic channels,[26,27] is usually used in complicated microfluidic channels; however, the printing ability was limited by low resolution and the restriction in materials.[28] Laser-based processes are considered as a more accessible technique, but expensive and inflexible.[29] In recent years, friction-induced selective etching, consisting of tip scanning and selective etching, is employed for fabricating micro/nanochannels that have broken through the limits of conventional lithographic diffraction and achieved one-atom depth, and provides conveniences in realizing cross-scale chips.[30] It was found that amorphous silicon (a-Si) generated in the scratching can resist the etching in acid or alkaline etchant, while other crystal defects including dislocations and lattice distortions can facilitate the etching.[31] The

sequential atomic arrangement of Si lattice can be destroyed by the scratching, forming superficial a-Si atoms with dangling bonds. The a-Si layer can cause the increase in the required energy for removing a-Si atoms in alkaline solutions. In comparison, lattice distortions, e.g., dislocations and stacking faults, can widen the Si atom spacing and have more dangling bonds in {111} equivalent planes, facilitating the reactive species diffusing to the reaction interface and thereby initiating the rapid replacement reaction of H groups by OH groups.[31] Accordingly, effective control of the scratching process, that is, the control of crystal damage generation, can ensure the post etching-induced channels formed in the design way.

According to previous reports, it seems highly possible to achieve asymmetric channels with efficient mixing through scanning probe lithography (SPL) and selective etching. In this study, misaligned sine micromixers with depth variation and phase difference (Φ) were designed and fabricated. Sinusoidal patterns with variable phase were created by SPL and then etched in KOH-based solution to obtain the depth-variable channels. The fabrication mechanism was addressed based on experimental detections and numerical simulations. The mixing performance was tested with two fluids, which was further verified by simulations. A replicable process was also conducted for the micromixer.

2. Materials and methods

2.1. Materials

Single-sided polished B-doped Si (100) wafers covered with 20 nm-thick Si_3N_4 film were applied as substrate materials. All the Si wafers were supplied by Suzhou Research Materials Microtech Co., Ltd., China, and the root mean square (RMS) roughness was measured as no more than 0.1 nm by a conductive atomic force microscopy (AFM; E-Sweep, Hitachi Instruments Inc., Japan). Before the fabrication, the Si wafers were ultrasonically cleaned successively for 5 min with acetone and alcohol. The polydimethylsiloxane (PDMS) was prepared in standard protocol where the elastomer and its crosslinker (Sylgard 184, Dow Corning, USA) were mixed in a 10:1 ratio (by weight). The homogeneous mixture of elastomer and crosslinker was placed in a vacuum desiccator for degassing, and then heated for curing (70 °C, 4 h). The cured PDMS was cut into the same size as the Si wafer and perforated in alignment with the inlets of Si channel. AFM images were obtained by a Si_3N_4 tip (MSCT, Veeco Instruments Inc., USA) with a spring constant of 0.1 N/m. The distribution of a-Si in scratching was detected by Raman spectrum (Lab RAM HREvolution, Horiba, Japan).

2.2. Methods

As shown in Fig. S1, a sinusoidal channel pattern with phase difference and square inlets on Si wafer coated with 20 nm-thick Si_3N_4 film was scratched by a diamond tip

under applied normal force of 30 mN. Based on pretests, the force 30 mN was enough for the diamond tip to penetrate the Si_3N_4 film in the scratching. Next, the Si wafer with misaligned structure was etched in a mixture of 20 wt% KOH and isopropyl alcohol (IPA) at 50 ^{o}C for 4 h to obtain deeper channel. KOH solution was chosen as the etchant because of the excellent selective etching of Si_3N_4-coated Si substrate and low toxicity. Following this, it was placed on a petri dish together with pre-prepared PDMS for oxygen plasma treatment, where parameters included radio frequency power (18 W) and plasma treatment time (3 min). There silanol (Si-OH) groups exist on the surface of PDMS and Si wafers after plasma treatment, which can produce a hydrophilic surface and increase its surface free energy (SFE).[32] This surface modification leads to irreversible bonding with Si-based substrates, through siloxane covalent bonds (Si-O-Si), providing a simple and stable bonding procedure and guaranteeing to seal of the mixer.[32] Finally, red and green dyes were introduced into the mixer with a syringe from two separate inlets, at a flow rate of 1.08 ml/min. Meanwhile, the real-time mixing was observed by the microscope.

3. Results and discussion

3.1. Channel design

Asymmetric structures, mentioned in many studies, are conducive to the mixing.[19,21] Therefore, misaligned sine structures with phase difference are optimized from general sine channels in this study, as shown in Fig. 1. The sine curve equations of two side

walls in general sine micromixers were coordinated, while misaligned sine micromixers were designed with a phase difference. Two fluids can be introduced by the straight channel and flow into the sinusoidal channel for mixing. The length and width of the sinusoidal channels are L = 3000 μm and *w* = 50 μm, respectively.

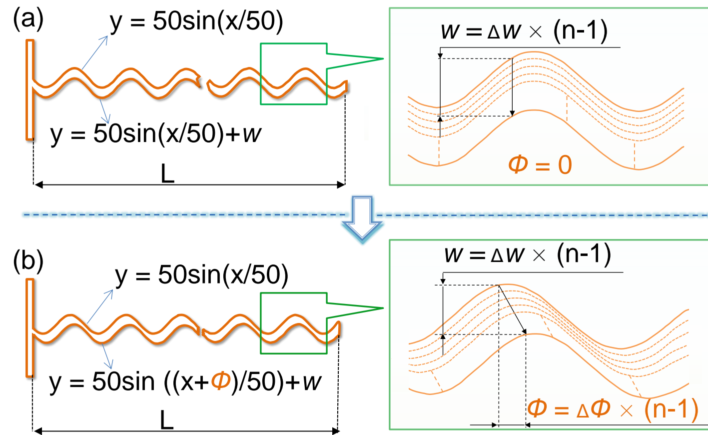

Fig. 1 The designed sinusoidal micromixer schematic. (a) General sine micromixer. (b) Misaligned sine micromixer. The n means the number of traces.

The mixing efficiency of channels with phase difference (Φ = 0, 5, 10, 15, 20, and 25 μm) were numerically simulated by COMSOL software. Here, $\Phi = 0$ was the general sine channel, while Φ = 30 μm was a clogged channel. In numerical simulation, temperatures, densities, dynamic viscosities, and diffusion coefficient were 293.15 K, 9.97 Kg/m^3, 8.978e^{-4} Pa·s, and 5e^{-11} m^2/s respectively. The flow velocities of the fluid passing through two inlets were 30 mm/s, but the concentrations were 0 and 1 mol/m^3, respectively. According to the Reynolds equation, the Reynolds number in two entrances was 0.3445, which is within the range of laminar flow.[8]

The liquid is assumed as steady incompressible Newtonian laminar flow and the model is governed by steady equations, Navier-Stokes equations, and Convection-Diffusion equations.[33] The mixing index (*MI*) of two-phase flow is calculated by concentrations taken at a cross section of the sinusoidal channel. To sure the calculation accuracy, 500 sample points are evenly taken. The value of the *MI* is between 0 and 1, where 1 means complete mixing and 0 means no mixing at all, and the larger the value of *MI*, the better the mixing efficiency.[21]

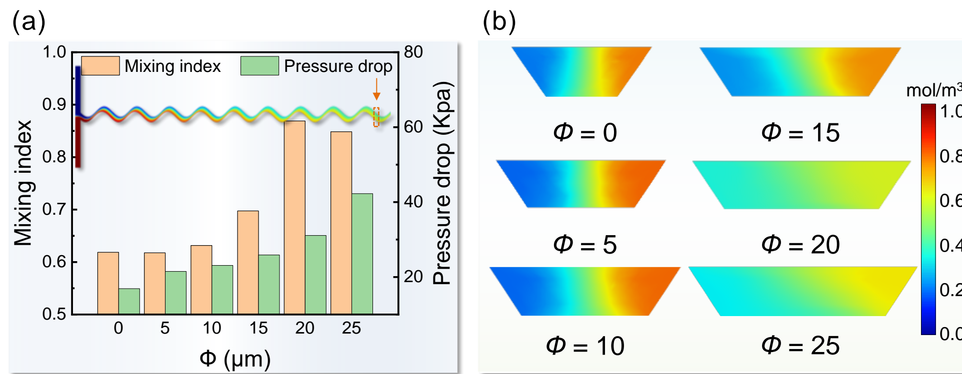

Fig. 2 Optimization of the phase difference in misaligned sine micromixers. (a) Mixing index and pressure drop of misaligned sine micromixers. (b) Cross-sectional snapshots at the tail of misaligned sine micromixers.

The mixing efficiency of channels with various phase difference is simulated in the same boundary condition. The cross-sectional *MI* at the tail of misaligned micromixers varies with the phase difference, as shown in Fig. 2(a), and cross-sectional snapshots are shown in Fig. 2(b). It can be noted that the misaligned sine channel with Φ = 20 μm presents the maximum *MI*, while the one with Φ = 25 μm features the

maximum pressure drop. Considering both pressure drop and mixing efficiency, the sine channel with Φ = 20 μm is selected for further investigations.

3.2. Channel fabrication

As shown in Fig. S1(a), the sliding traces with Φ = 20 μm were designed for the scratching and post-etching. During the selective etching, the etching rate of Si_3N_4 in KOH etchants is much slower than the monocrystalline Si, and hence the channel appeared in-situ from the scratched area.[34] From the microscope images of channels shown in Fig. 3, it is noted that the depth of the sinusoidal channel varies regularly along the scratching traces.

The depth of cross sections A-A, B-B, and C-C in the sinusoidal channel detected by the profilometer are about 22, 29, and 29 μm, respectively, as shown in Fig. 3(f). The shape of cross section A-A is a triangle, different from the trapezoidal B-B and C-C. The sinusoidal channel presents a thick-thin alternate structure, and its 3D schematic diagram is presented in Fig. 3(e). Correspondingly, some similar sinusoidal channels with different widths (w = 10, 20, 30, and 40 μm) were fabricated using the above designing, as shown in Fig. S2(g). By comparing the depth, it can be seen that cross section A-A is the shallowest, while C-C is the deepest. Cross-section channel shapes vary with the width, and the trapezoidal are more likely to appear in wider channels. As a result, the misaligned channels were obtained with both depth variation and phase difference. The formation of the straight outside of the sine channel can be ascribed to

the undercut during the etching. The break bond density of Si atoms at the convex corner is higher than that on the (111) plane, and the convex corner can be rapidly etched in alkali solution.[35] In addition, the etch rate of some typical crystal planes, e.g. (110) and (100), is faster than the (111) plane, forming the terminate plane (111) as the straight outside.[36]

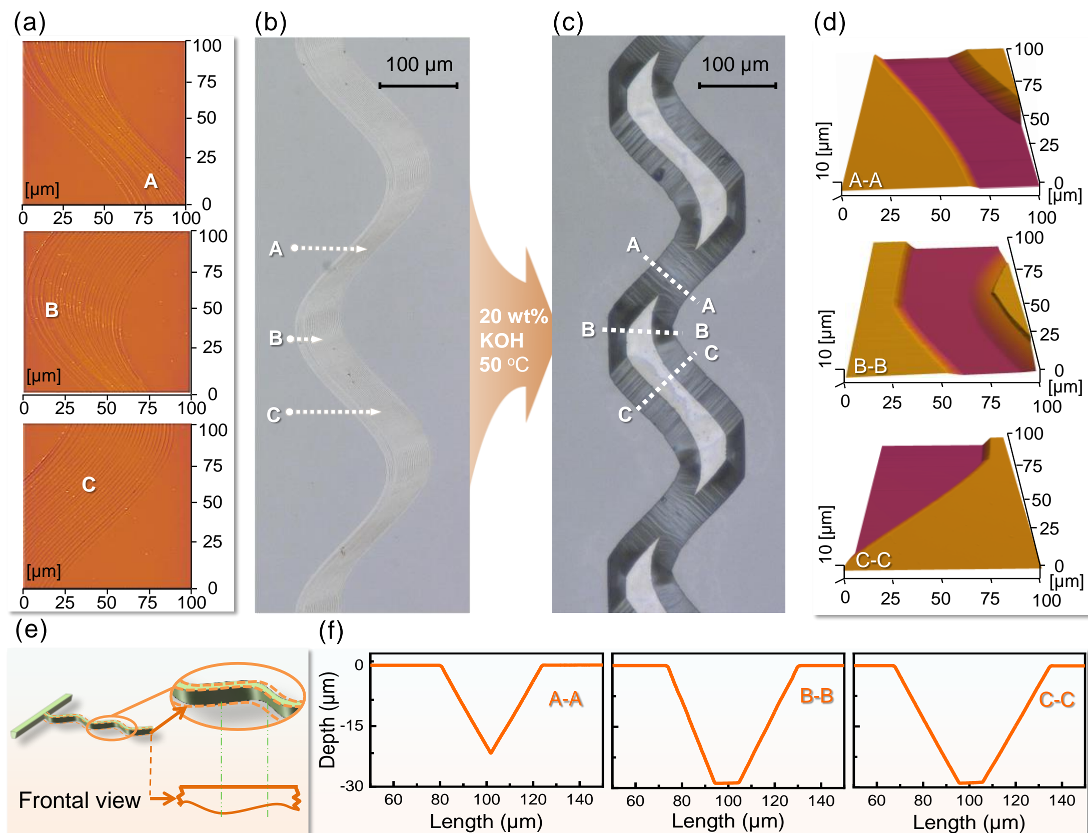

Fig. 3 Fabrication of sinusoidal channels. (a) AFM images of scratching sine traces. (b) Microscope image of scratching sine traces. (c) The sinusoidal channel stemming from the etching. (d) AFM images of the sinusoidal channel. (e) 3D sketch of the sinusoidal channel in (c). (f) Cross-section profiles measured from the marked A-A, B-B, and C-C positions with a profilometer, where the measurement of the profiles was schematically indicated on the left.

3.3.1. Fabrication mechanism: Distribution and formation of a-Si

Since the misaligned channels with both depth variation and phase difference can be obtained under scratching and post-etching, roles of scratch-induced crystal deformations (a-Si, distorted Si, and nanocrystals) in KOH etchant can be regarded as the main contributor to the structure formation.[31,37] Therefore, by controlling the generation of a-Si, it is possible to control selective etching and further obtain delicate structures. Here, experimental and simulation are employed to depict the process for a-Si generation during the tip scratching.

Fig. 4(a) displays four Raman spectra collected on areas A, B, and C, as well as original monocrystalline Si surface. On the overall spectra, single bands at 520 cm^{-1} and around 480 cm^{-1} can be observed, which can be assigned to optical modes of bulk Si (Si-I) and a-Si. [38,39] Comparing the four spectra, it can be concluded that the a-Si layer at point A is the thickest, followed by B and the thinnest at C. Meanwhile, a part of scratching traces had been detected by Raman imaging microscope, and the result was shown in Fig. 4(b). The color gradually changes from red to blue with the pattern becoming wider, which indicates that the area of Raman peak band in the range of 450 cm^{-1} - 510 cm^{-1} decreased. From Fig. 3(a) and 3(b), it's obvious that the span between adjacent scratch traces gets narrower from area A to C. This could be speculated that the existence of a-Si structure is reduced with the increase of the line span for the scratching. Parallelly, from the stress simulation for the scratches, it's obvious that area A bears more occasions of stress applied due to a narrow overlapped scratching, as

shown in Fig. 5(a) and 5(b). Therefore, a thicker a-Si layer was detected in area A. By contrast, the wider scratch traces and less overlapped stress provide a thinner a-Si layer in area B and especially in C. Therefore, it is concluded that thicker a-Si layer could be obtained by reducing the line spacing in the scratching.

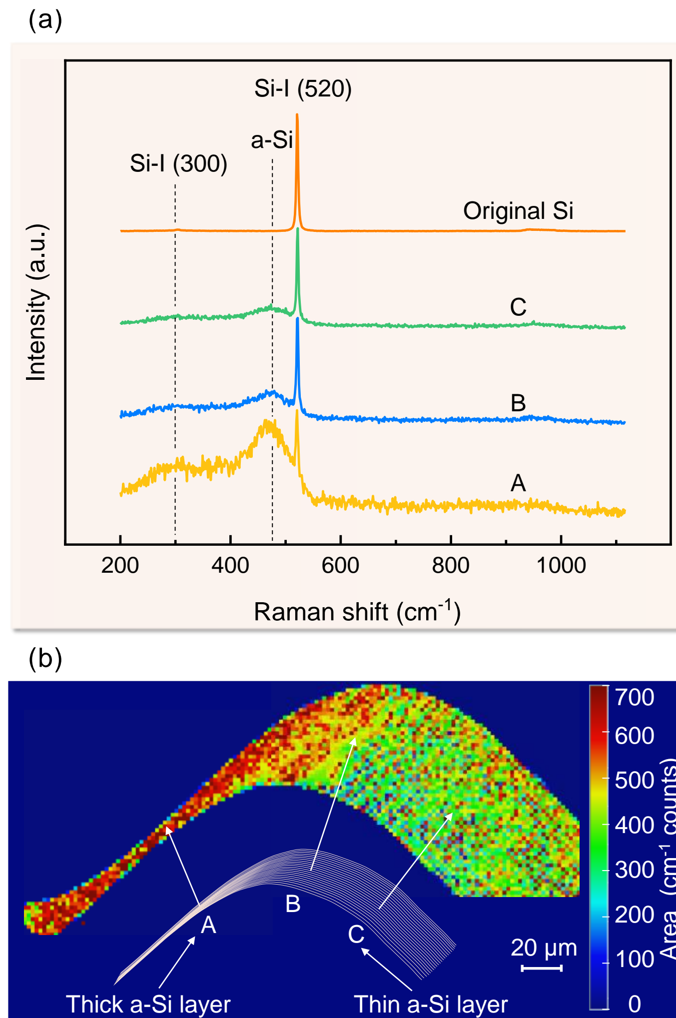

Fig. 4 Raman detections of the sine scratch (before etching). (a) Raman spectra on different sites on the scratch. (b) Raman mapping of the partial surface of the scratch traces. The inset shows the scratching sine traces.

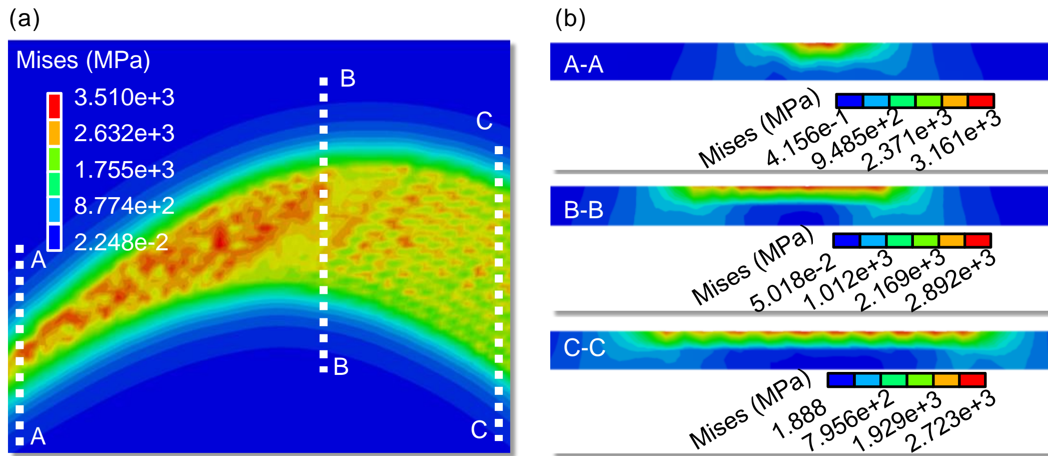

Fig. 5 Stress distribution of the scratched area with varied spans. (a) Stress distribution of partial sinusoidal scratch. (b) Stress distribution of cross sections A-A, B-B, and C-C, corresponding to that in Fig. 4(b).

3.3.2. Fabrication mechanism: Role of a-Si in selective etching

During the scratching, the ordered Si lattice can be destroyed and transformed to a-Si, leading to higher energy required for etching off in alkaline solutions.[31] According to the content or thickness of a-Si layer (Fig. 4), it can be inferred that the rank of the required energy for surface removing, from the most to the least, is area A, B, and C, which corresponds to etching rate from the slowest to the fastest, respectively. In addition, Si_3N_4, serving as a powerful protect mask in KOH etchant,[34] is still on the un-scratched region of the wafer, while a-Si, acting as a relatively weak mask,[29] is distributed in the scratched area. Evidently, the etching rate of the scratches with sine channel patterns is faster than that of other area. It is worth stating that a-Si plays an anti-etching role only in the early etching stage. After a-Si is etched off, the depth

variation in channels is already faintly visible, and then the distorted Si below acts as an etching promoter, accelerating the formation of deeper channels. In the later stage of etching, crystal deformations are exhausted in the alkaline solution, and the stable 54.74^{o} angle between crystalline surface (111) and (100)[40] determined that the cross-sectional shapes of the channels are triangle or trapezoidal. As a result, benefiting from the different thickness of a-Si generated by the scratches, the variable depth of misaligned channels can be obtained after the selective etching.

3.4. Mixing performances

According to the analysis for the structures, the misaligned mixer featured with depth variation and phase difference (D-P mixer) may bring about higher mixing efficiency than the one with phase difference only (P mixer). Therefore, the mixing performances of the two sinusoidal micromixers (P mixer and D-P mixer) were compared by numerical simulations and analyzed through flow velocities and streamlines. Fig. 6(a) displays the concentration distribution at three given positions along the two micromixers. It can be seen that the color distribution of the D-P mixer at 2.9 mm is more even than the P mixer. Again, as shown in Fig. 6(b), the *MI* of the P mixer at 3 mm is 0.871, while the same *MI* appears at 2.4 mm for the D-P mixer, which proves better mixing behavior of the latter. As shown in Fig. 6(c), the front and top views of streamline diagram for the two micromixers show that more chaotic flow lines exist in the D-P mixer, while regular flow lines exist in the P mixer. The flow velocities in cross

section C-C are nearly the same for both channels, while faster flow velocity was detected on cross section A-A of the D-P mixer, as shown in Fig. 6(d). As a result, the variable cross section shape accelerates flow velocity changing, making it more likely to produce secondary flow and increase the intensity of convection, and thereby higher mixing efficiency was assigned to the misaligned sine channel with both depth variation and phase difference.

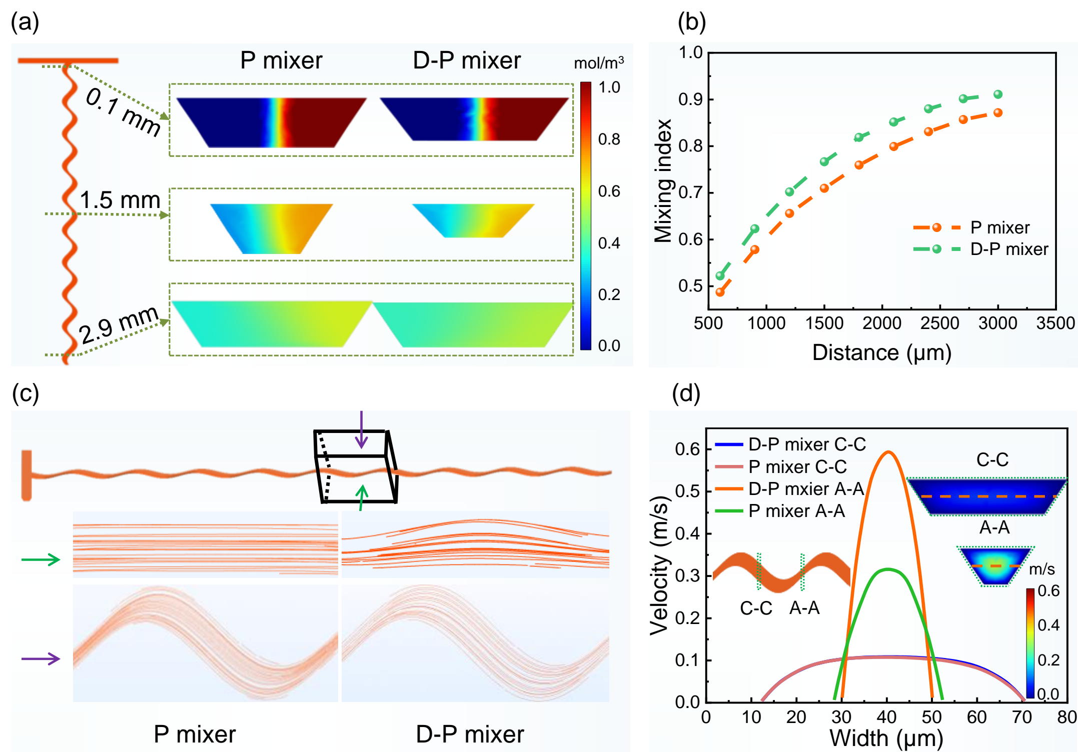

Fig. 6 Numerical simulations of two misaligned sine channels. (a) Concentration distribution at three given positions of the two mixers. (b) *MI* of different positions along the length of two mixers. (c) Streamlines at the same position of the two mixers. (d) Flow velocities in cross sections A-A and C-C of the two mixers.

For further instigating the mixing performance, mixing performance was experimentally tested for the packaged micromixer with the misaligned sine channel

with depth variation and phase difference. Red and green dyes were introduced into the inlets by digital syringe pumps at a flow rate of 1.08 ml/min and mixed in the sinusoidal channel. Fig. 7(a) shows the snapshots of the mixing process by the simulation. For comparison, the image of mixing process in the channel was captured with a microscope and converted into the RGB format (Fig. 7(b)). Then the data for the mixing was extracted from its pixel. The intensity of the captured image was normalized and the standard deviation was calculated from its mean values.[2] The *MI* from the experiment and simulation was calculated and shown in Fig. 7(c). It is found that there is a consistency between the experiment and simulation. It is worth noting that the difference in Fig. 7(c) may be ascribed to the incomplete matching of bottom wall in the channel between the actual and simulated, and the measurement error for the dye fluid image. As a result, the misaligned sine micromixer fabricated in this study presents ultra-higher mixing efficiency than ever, which promotes the miniaturization of high-performance microfluidic chips.

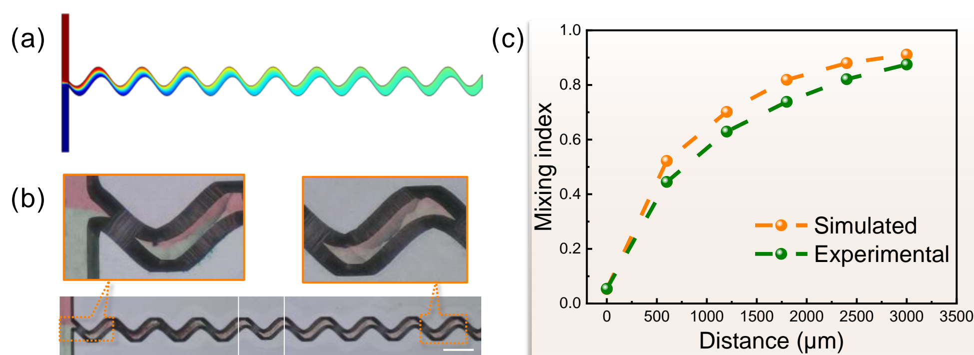

Fig. 7 Experimental and simulated mixing efficiency of the misaligned micromixer with both depth variation and phase difference. (a) Snapshots of mixing simulated. (b) Snapshots of two dyes mixing. The scale bar is 200 μm. The sinusoidal channel is a

patchwork of three images. (c) Mixing index of experiment and simulation.

It is worth mentioning that the fabricating process of misaligned sine channels by diamond tip scratching and wet etching on Si substrates is well reproducible, yet time-consuming. Considering the low efficiency of the scratching and post-etching, the sine channel on Si wafer can be employed as a template for consistent manufacturing. Here, a strategy is proposed to duplicate complex channels from Si substrate to PDMS surface, permitting the production with high efficiency and low cost, as shown in Fig. S3. This method is also expected to enable the fabrication of large-area functional microstructures on PDMS or related materials surface.

4. Conclusions

In this study, to increase the mixing efficiency, misaligned channel was designed based on general sine channel, and the optimal phase difference (Φ = 20 μm) was obtained by using simulations. Then the misaligned sine patterns with phase difference were created by SPL and the variable depth channel was completed by selective etching in KOH-based solution. Experimental tests showed that different solutions were nearly completely mixed in the fabricated micromixer within 3 mm, and such excellent performance was confirmed by numerical simulations. Further study showed that thicker a-Si layer was obtained by reducing the line spacing in the scratching, which was confirmed by Raman detections and stress simulations. It is deduced that the formation of the misaligned channels is mainly attributed to the anti-etching

performance of a-Si generated by the designed scratching. For saving the cost and time in fabricating the misaligned channel, a high-precision replicable process was also presented for the micromixer duplicate, shedding much light on mass production. The study provided opportunities for promoting the miniaturization of high-performance microfluidic chips and offered a practical guide for applications.

Authors contribution

Tingting Chen: conceptualization, software, formal analysis, investigation, methodology, validation, visualization, writing – original draft, writing – review & editing. Licong Cui: investigation, methodology, validation. Wang He: investigation, validation, visualization. Renxing Liu: methodology. Chengqiang Feng: formal analysis. Lei Wu: investigation. Yang Wang: supervision. Huiyun Liu: supervision. Linmao Qian: supervision. Bingjun Yu: conceptualization, software, formal analysis, investigation, methodology, validation, visualization, writing – original draft, writing – review & editing, supervision, funding acquisition.

Conflicts of interest

No conflicts to declare.

Acknowledgments

This study is supported by the National Natural Science Foundation of China (52175549).

References

1 A. Afzal and K. Y. Kim, *Chem. Eng. J.*, 2015, 281, 134-143.

2 I. Shah, S. W. Kim, K. Kim, Y. H. Doh and K. H. Choi, *Chem. Eng. J.*, 2019, 358, 691-706.

3 S. J. Kim, F. Wang, M. A. Burns and K. Kurabayashi, *Anal. Chem.*, 2009, 81, 4510-4516.

4 Y. W. Shi, Y. Cai, Y. H. Cao, Z. Y. Hong and Y. F. Chai, *Trac-Trend Anal. Chem.*, 2021, 134, 20.

5 M. Ripoll, E. Martin, M. Enot, O. Robbe, C. Rapisarda, M. C. Nicolai, A. Deliot, P. Tabeling, J. R. Authelin, M. Nakach and P. Wils, *Sci. Rep.*, 2022, 12, 12.

6 S. J. Haswell, *Nature*, 2006, 441, 705-705.

7 R. Dylla-Spears, T. D. Yee, K. Sasan, D. Nguyen, N. A. Dudukovic, J. M. Ortega, M. A. Johnson, O. D. Herrera, F. J. Ryerson and L. L. Wong, *Sci. Adv.*, 2020, 6, 7.

8 J. Knoska, L. Adriano, S. Awel, K. R. Beyerlein, O. Yefanov, D. Oberthuer, G. E. P. Murillo, N. Roth, I. Sarrou, P. Villanueva-Perez, M. O. Wiedorn, F. Wilde, S. Bajt, H. N. Chapman and M. Heymann, *Nat. Commun.*, 2020, 11, 12.

9 T. J. Ober, D. Foresti and J. A. Lewis, *Proc. Natl. Acad. Sci. U. S. A.*, 2015, 112, 12293-12298.

10 G. Z. Cai, L. Xue, H. L. Zhang and J. H. Lin, *Micromachines*, 2017, 8, 27.

11 A. Banerjee and A. K. Nayak, *J. Non-Newtonian Fluid Mech.*, 2019, 269, 17-27.

12 R. Kamali, S. A. Shekoohi and A. Binesh, *Nano-Micro Lett.*, 2014, 6, 30-37.

13 S. Park, H. S. Chuang and J. S. Kwon, *Sens. Actuators, B*, 2021, 329, 10.

14 X. Y. Chen and H. Lv, *Sci. Rep.*, 2022, 12, 17.

15 S. Kim, Y. H. Joung, S. Ahn, C. Park, J. Choi and C. Koo, *Lab Chip*, 2020, 20, 4474-4485.

16 H. Shi, Y. Zhao and Z. Liu, *Sens. Actuators, B*, 2020, 321, 11.

17 J. Wang, N. Zhang, J. Chen, V. G. J. Rodgers, P. Brisk and W. H. Grover, *Lab Chip*, 2019, 19, 3618-3627.

18 K. Y. Hsiao, C. Y. Wu and Y. T. Huang, *Chem. Eng. J.*, 2014, 235, 27-36.

19 A. Haghighinia and S. Movahedirad, *Int. J. Heat Mass Transfer*, 2019, 139, 907-916.

20 C. Y. Lee, W. T. Wang, C. C. Liu and L. M. Fu, *Chem. Eng. J.*, 2016, 288, 146-160.

21 A. Haghighinia and S. Movahedirad, *Anal. Chim. Acta*, 2020, 1098, 75-85.

22 L. Bai, Y. H. Fu, M. Yao and Y. Cheng, *Chem. Eng. J.*, 2018, 332, 537-547.

23 H. M. Xia, J. W. Wu, J. J. Zheng, J. Zhang and Z. P. Wang, *Lab Chip*, 2021, 21, 1241-1268.

24 M. K. Parsa, F. Hormozi and D. Jafari, *Comput. Fluids*, 2014, 105, 82-90.

25 B. Mondal, S. K. Mehta, P. K. Patowari and S. Pati, *Chem. Eng. Process*, 2019, 136, 44-61.

26 J. B. Nielsen, R. L. Hanson, H. M. Almughamsi, C. Pang, T. R. Fish and A. T.

Woolley, *Anal. Chem.*, 2020, 92, 150-168.

27 V. Mehta and S. N. Rath, *Bio-Des. Manuf.*, 2021, 4, 311-343.

28 A. G. Niculescu, C. Chircov, A. C. Birca and A. M. Grumezescu, *Int. J. Mol. Sci.*, 2021, 22, 26.

29 A. L. Jauregui, H. R. Siller, C. A. Rodriguez and A. Elias-Zuniga, *Int. J. Adv. Manuf. Technol.*, 2010, 48, 963-972.

30 L. Wu, K. D. Shang, T. T. Chen, C. Q. Feng, T. T. Yang, Z. J. Zhao, B. J. Yu and L. M. Qian, *Sens. Actuators, B*, 2022, 372, 9.

31 L. Wu, L. C. Cui, W. He, J. Guo, B. J. Yu and L. M. Qian, *ACS Appl. Mater. Interfaces*, 2022, 14, 29366-29376.

32 K. Y. Song, H. B. Zhang, W. J. Zhang and A. Teixeira, *Microfluid. Nanofluid.*, 2018, 22, 9.

33 J. X. Zhang and X. P. Luo, *Micromachines*, 2018, 9, 18.

34 J. Guo, B. J. Yu, X. D. Wang and L. M. Qian, *Nanoscale Res. Lett.*, 2014, 9, 7.

35 W. Dong, X. D. Zhang, C. X. Liu, M. Li, B. K. Xu and W. Y. Chen, Microelectronics Journal, 2004, 35 (5), 417-419.

36 J. Guo, B. J. Yu, X. D. Wang and L. M. Qian, Nanoscale Res. Lett., 2014, 9, 7.

37 D. Findley, M. Page, M. Al-Jassim, D. L. Young, P. Stradins and S. Agarwal, *ACS Appl. Mater. Interfaces*, 2019, 11, 42021-42031.

38 S. Ruffell, J. E. Bradby and J. S. Williams, *Appl. Phys. Lett.*, 2006, 89, 3.

39 A. Kailer, Y. G. Gogotsi and K. G. Nickel, *J. Appl. Phys.*, 1997, 81, 3057-3063.

40 A. S. Kale, W. Nemeth, H. Guthrey, S. U. Nanayakkara, V. LaSalvia, S. Theingi,

A. R. Gao, N. Lu, P. F. Dai, T. Li, H. Pei, X. L. Gao, Y. B. Gong, Y. L. Wang and C. H. Fan, *Nano Lett.*, 2011, 11, 3974-3978.